A scale-space medialness transform based on boundary concordance voting

Xu, Ming; Pycock, David

DOI:
10.1023/A:1008312821522

Document Version
Early version, also known as pre-print

Citation for published version (Harvard):
Xu, M & Pycock, D 1999, 'A scale-space medialness transform based on boundary concordance voting', *Journal of Mathematical Imaging and Vision*, vol. 11, no. 3, pp. 277-299. https://doi.org/10.1023/A:1008312821522

To appear in *Journal of Mathematical Imaging and Vision*

A Scale-Space Medialness Transform Based on Boundary Concordance Voting

Ming Xu and David Pycock

School of Electronic and Electrical Engineering
University of Birmingham
Birmingham, B15 2TT, UK
E-mail: xum@eee.bham.ac.uk D.Pycock@bham.ac.uk

ABSTRACT

The Concordance-based Medial Axis Transform (CMAT) presented in this paper is a multiscale medial axis (MMA) algorithm that computes the medial response from grey-level boundary measures. This non-linear operator responds only to symmetric structures, overcoming the limitations of linear medial operators which create "side-lobe" responses for symmetric structures and respond to edge structures. In addition, the spatial localisation of the medial axis and the identification of object width is improved in the CMAT algorithm compared with linear algorithms. The robustness of linear medial operators to noise is preserved in our algorithm. The effectiveness of the CMAT is accredited to the concordance property described in this paper. We demonstrate the performance of this method with test figures used by other authors and medical images that are relatively complex in structure. In these complex images the benefit of the improved response of our non-linear operator is clearly visible.

Keywords: Image analysis, medial axis, multiscale, shape representation.

1 INTRODUCTION

Accurate and robust shape representation is important as a basis for image interpretation in a wide range of computer vision applications. To be accurate and robust, a shape representation should describe both local and global features. The Medial Axis Transform (MAT) [1] achieves this by generating an axis that is the locus of the centres of the maximal disks that can be inscribed within an object. These loci are also labelled with the radius of the maximal disk. The MAT provides a direct encoding of local properties of object shape, such as edge orientation and curvature, and of global properties, such as overall length and orientation. Another attractive property of the MAT is that the branching structure of the object is reflected by the branching of the axis. This yields a natural correspondence between components of the object and the shape description.

One problem with the MAT is that small boundary variations can greatly disturb the medial axis structure of the primary shape. There is also no indication concerning the relevance of these axial components to the structural description of the shape. Using multiscale analysis to establish a hierarchical MAT representation the relative importance of the medial axis at each scale can be described [12]. Descriptions of detailed aspects of form (and noise) are provided in the higher resolution levels of the hierarchy and do not disturb the description at lower resolution levels. Such a hierarchical representation supports model-driven schemes of interpretation [15]. To perform multiscale analysis a series of smoothing steps must be taken. "Smoothing" can be applied to the local curvature of an object contour or to the image intensity. Koenderink [6] argued that filtering images to create a scale-space representation captures global relationships better than contour smoothing. Moreover, this

approach does not need a prior segmentation and avoids important boundary information being discarded at an early stage of processing. Pizer's Multiscale Medial Axis (MMA) [13] is a robust object representation scheme [11] that has been applied in image registration [4].

The Multiscale Medial Axis, referred to above, is identified as a ridge in medialness space and medialness as a measure of the likelihood that a given location is a symmetric point at that scale. This definition of the MMA improves the multi-resolution graphical scheme of Crowley and Parker [2] by providing better ridge definition and quantitative representation.

Medialness can be computed by convolving grey-scale images with different sizes of DoG [2] or LoG kernels [4]. Axis-centred operator, such as these, respond well at a scale and position where the operator optimally engages two sides of an object. Medialness can also be computed by accumulating the response of directional Gaussian derivatives around a circle, with a radius proportional to scale. One example of this approach is the Hough-like Medial Axis Transform (HMAT) [8]. This boundary-centred operator is less sensitive to variations within an object, less sensitive to differences in boundary contrast and more adaptable than axis-centred operators [9]. Once the medialness scale-space is obtained, the MMA can be extracted using the definition of "maximum convexity ridge" [3][5] or "optimal scale ridge" [4][12]. These two methods produce qualitatively similar results [14].

Both the HMAT and LoG algorithms use linear medialness operators which are data independent and can be computed as a linear convolution of a radially symmetric kernel with the image. They are not only sensitive to symmetric structures, but also respond to edge structures. Even for symmetric structures, they generate two side lobes of opposite sign to the main response. These create "spurious" medialness responses that are not associated with any structural symmetry. The result of linear operators is a mixture of boundary and medial

characteristics. When multiple figures are present in an image processed using such linear operators the addition of boundary related responses to the medial responses produces a confused result. To overcome the limitation of linear filtering the boundary responses of two putative edges must be combined in a non-linear way. In previous work this was performed for multiscale line detection using the minimum [7][15] and for fixed-scale MAT of grey-level images using the product [18]. Morse [9][10] refined the result of the HMAT through an iterative voting phase, called credit attribution. In this scheme boundary votes were re-allocated in proportion to the agreement among weighted boundary votes in the previous iteration. This is an enhancement process and cannot overcome the fundamental failing of the linear operator used. The iterative nature of the credit attribution scheme also makes it computationally expensive.

In this paper, we propose a Concordance-based Medial Axis Transform (CMAT), which considers both the symmetry of boundary positions and the symmetry of boundary strength. The non-iterative CMAT algorithm avoids the spurious responses generated by linear operators, provides better localisation of the medial axis and a response that more clearly identifies object width.

In Section 2, we describe the computation of the CMAT algorithm. In Section 3, the concordance property which expresses the symmetry of boundary strength is described and discussed. In Section 4, we present quantitative results of the performance of the CMAT algorithm and compare it with selected linear medial operators; Results of the application of the CMAT to synthetic and natural images are also presented and compared in this section.

2 THEORY AND COMPUTATION

2.1 Concordance-based Medial Axis Transform

2.1.1 Definition for continuous co-ordinates

The boundariness scale-space of the original image, $I(\mathbf{x})$, is defined as:

$$\mathbf{B}(\mathbf{x},\sigma) = I(\mathbf{x}) * \sigma\nabla G(\mathbf{x},\sigma) \tag{1}$$

where $\mathbf{x} = (x_1,\ldots,x_n)^T \in R^n$ denotes spatial position in an n-dimensional superplane; G is the n-dimensional Gaussian kernel with unit volume:

$$G(\mathbf{x},\sigma) = \frac{1}{(2\pi\sigma^2)^{n/2}} e^{-\mathbf{x}^T\mathbf{x}/2\sigma^2}$$

and $\sigma \in R^+$ is the scale. The boundariness response can be jointly represented by the gradient magnitude:

$$b(\mathbf{x},\sigma) = \left\|\mathbf{B}(\mathbf{x},\sigma)\right\| \tag{2}$$

and a unit gradient vector:

$$\hat{\mathbf{n}}(\mathbf{x},\sigma) = \frac{\mathbf{B}(\mathbf{x},\sigma)}{\left\|\mathbf{B}(\mathbf{x},\sigma)\right\|} \tag{3}$$

For each point $\mathbf{x}$ in boundariness space, the initial contribution, $b(\mathbf{x},\sigma)$, to medialness space is made at:

$$\mathbf{y} = \mathbf{x} + r\hat{\mathbf{n}}(\mathbf{x},\sigma) \tag{4}$$

where $\mathbf{y} \in R^n$ is the n-dimensional spatial position in medialness space, and $r = k\sigma$ (k is the ratio of radius to scale, see Fig.1).

The integration of initial contributions in medialness space provides the initial medialness response. Written as a Radon Transform [16], this is:

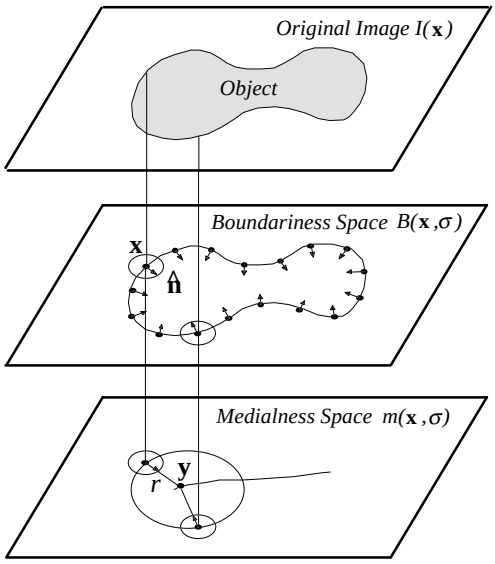

Figure 1: The medialness response is the integration of boundariness contributions.

$$m_0(\mathbf{y},\sigma) = \int_{R^n} b(\mathbf{x},\sigma)\delta(\mathbf{y}-\mathbf{x}-r\hat{\mathbf{n}}(\mathbf{x},\sigma))d\mathbf{x} \tag{5}$$

where the Delta function is defined as $\int_{R^n}\delta(\mathbf{x})d\mathbf{x}=1$ and $\delta(\mathbf{x})=0$ when $\mathbf{x}\neq\mathbf{0}$. In two dimensional space, the initial medialness at **y** is the integration of directional Gaussian derivatives around a circle centred at **y** with radius r; the orientation of the Gaussian derivatives being towards the centre of the circle, see Fig. 1. This definition is close to Blum's MAT [1] and the HMAT [8].

The initial medialness has high values for symmetric structures but also responds to edge structures because the boundariness response, $b(\mathbf{x},\sigma)$, for an isolated edge results in the medialness response, $m_0(\mathbf{y},\sigma)=b(\mathbf{x},\sigma)$. To obtain a medialness response that is sensitive only to symmetric edges, the contribution to medialness from boundariness is constrained by a weighting, $p(\mathbf{x},\sigma)$, called *contribution confidence*. The requirements for contribution confidence are:

(1) The medialness response should not be greater than the initial medialness response, i.e. $0 \le p(\mathbf{x},\sigma) \le 1$.

(2) A single boundary produces no medialness response, i.e.:

$p(\mathbf{x},\sigma) = 0$ *if* $m_0(\mathbf{y},\sigma) = b(\mathbf{x},\sigma)$.

(3) The greater the initial medialness, $m_0(\mathbf{y},\sigma)$, the more possible it is for **x** to contribute to medialness, provided $m_0(\mathbf{y},\sigma) > b(\mathbf{x},\sigma)$. Therefore $p(\mathbf{x},\sigma)$ increases with $m_0(\mathbf{y},\sigma)$.

The definition of contribution confidence used here is:

$$p(\mathbf{x},\sigma) = \frac{m_0(\mathbf{y},\sigma) - b(\mathbf{x},\sigma)}{m_0(\mathbf{y},\sigma)} \tag{6}$$

This measure of contribution confidence can be considered to be an estimate of the extent to which one boundariness point contributes to existing evidence of medialness. Using this confidence measure the boundariness contribution to true medialness is:

$$\mathbf{C}(\mathbf{x},\sigma) = \mathbf{B}(\mathbf{x},\sigma)\, p(\mathbf{x},\sigma) \tag{7}$$

The magnitude of such contributions is:

$$c(\mathbf{x},\sigma) = \left\| \mathbf{C}(\mathbf{x},\sigma) \right\| \tag{8}$$

The medialness response is the integration of boundariness contributions to true medialness:

$$m(\mathbf{y},\sigma) = \int_{R^n} c(\mathbf{x},\sigma)\delta(\mathbf{y} - \mathbf{x} - r\hat{\mathbf{n}}(\mathbf{x},\sigma))d\mathbf{x} \tag{9}$$

The estimation of confidence in Eq. (6) provides the "concordance" property of the Concordance-based Medial Axis Transform (CMAT), by which the medial response is high only when multiple boundaries jointly provide evidence of a symmetric structure. With this

formulation an isolated boundary cannot produce a medial response. This concordance property is analysed in section 3.

The definition of $\hat{\mathbf{n}}(\mathbf{x},\sigma)$ used in Eq. (4), (5) and (9) determines the medialness responses for dark objects (low grey-level value) on a light background (high grey-level value). The same equations can be used to compute the medialness response for the inverse phase (light object on a dark background) by inverting the sign of the unit vector $\hat{\mathbf{n}}(\mathbf{x},\sigma)$ such that:

$$\hat{\mathbf{n}}(\mathbf{x},\sigma) = -\frac{\mathbf{B}(\mathbf{x},\sigma)}{\left\|\mathbf{B}(\mathbf{x},\sigma)\right\|} \tag{10}$$

It is relatively simple to combine the computation of both sets of medialness either by summing absolute or signed values of medialness.

2.1.2 Computation in discrete space

For discrete spatial sampling, boundariness contributions to medialness space are typically distributed between grids. In order to improve the localisation of the medial axis, the real-values of the co-ordinates of boundariness contributions are preserved throughout the computation of medialness.

Let $\mathbf{m} \in I^n$ and $\mathbf{n} \in I^n$ be the discrete co-ordinates of points in n-dimensional boundariness and medialness spaces, respectively. Let $\mathbf{y} = (y_1,\ldots,y_N)^T \in R^n$ be the continuous co-ordinates of points in medialness space. Now we define a pseudo version of the discrete Delta function with real argument components: †

† The discrete Delta function is defined as : $\forall \mathbf{m} \in I^n, \delta(\mathbf{m}) = 1$ if $\mathbf{m} = 0$; otherwise $\delta(\mathbf{m}) = 0$.

$$\delta_p(\mathbf{y}) = \begin{cases} 1, & -1/2 \le y_i < 1/2, \quad i = 1, \ldots, n \\ 0, & otherwise \end{cases} \tag{11}$$

To estimate the contribution confidence of each boundariness point, **m**, the initial medialness at the corresponding position, **y,** in Fig. 1 must be known. This contribution is the summation of initial boundariness contributions over the unit volume centred at **y,** i.e. :

$$m_0(\mathbf{y}, \sigma) = \sum_{\mathbf{m}} b(\mathbf{m}, \sigma) \delta_p(\mathbf{y} - \mathbf{m} - r\hat{\mathbf{n}}(\mathbf{m}, \sigma)) \tag{12}$$

Likewise the boundariness contribution, $b(\mathbf{m}, \sigma)$, can be thought of as the accumulation of boundariness over a unit volume centred at **m**. The contribution confidence, $p(\mathbf{m}, \sigma)$, and the boundariness contribution, $c(\mathbf{m}, \sigma)$, are computed using Eq. (6) and Eq. (8). With discrete sampling, there are few boundariness points that contribute to medialness value at exactly the same position. To compensate for the sparseness of these contributions, a weighted summation over a volume is used in the computation of medialness response:

$$M(\mathbf{n}, \sigma) = \sum_{\mathbf{m}} c(\mathbf{m}, \sigma) G(\mathbf{n} - \mathbf{m} - r\hat{\mathbf{n}}(\mathbf{m}, \sigma), s) \tag{13}$$

Here G is the Gaussian kernel with the standard deviation s. This is similar to the procedure adopted in other medialness algorithms [10][19]. To construct the scale-space of the original image we can either solve the diffusion equation or apply Gaussian filter kernels of increasing size. The Gaussian filter is a linear diffusion process by which the response at a point in the original image is distributed over an area, the size of which changes linearly with scale. The standard deviation, s, of the Gaussian weighting function in Eq. (13) is chosen as $s = \lambda\sigma$ (λ is a proportionality constant). A Gaussian function is close to zero at a distance of more than three times its standard deviation. Therefore the radius of the volume influenced by a point is limited to 3s. This is illustrated for the 2-D case in Fig. 2. Point B in boundariness space

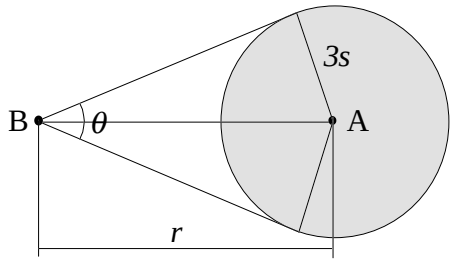

Figure 2: Point B in boundariness space contributes to medialness at point A. All similar contributions within a radius of *3s* of A are summed using a Gaussian weighting.

contributes to a circular area centred at A in medialness space. If we consider the weighted accumulation over an angular range θ, we have:

$$\theta = 2\sin^{-1}(3\lambda / k) \tag{14}$$

and θ is kept constant across scale.

The position argument in the Gaussian function of Eq. (13) is real-valued therefore it is not practical to construct a Gaussian look-up table indexed by position to accelerate computation. Instead, each boundariness contribution is distributed linearly between the four nearest neighbour grid points, in proportion to the distance to each neighbour, using:

$$m(\mathbf{n},\sigma) = \sum_{\mathbf{m}} c(\mathbf{m},\sigma) W(\left\|\mathbf{n} - \mathbf{m} - r\hat{\mathbf{n}}(\mathbf{m},\sigma)\right\|) \tag{15}$$

Here the distance weighting function W is defined as $W(d) = \max(1-d, 0)$; Other weightings are possible. The Gaussian weighting kernel is then applied to compute the final medialness response:

$$M(\mathbf{n},\sigma) = m(\mathbf{n},\sigma) * G(\mathbf{n}, s) \tag{16}$$

2.1.3 Algorithmic description of CMAT

In the computation of the CMAT a look up table (LUT) is used to identify the correspondence between medialness and boundariness points. An outline description of the CMAT algorithm is given in Fig. 3 and the computation of the LUT is described in the following section. The LUT contains a series of groups of boundariness points. The groups are identified in a second LUT.

1. For each scale σ
    1.1. For each discrete boundariness point compute the boundariness value using Eq. (1).
    1.2. For each discrete point in boundariness space compute the location of its contribution in medialness space using Eq. (4).
    1.3. Generate the association between each discrete medialness point and the group of contributing discrete boundariness points (see section 2.1.3.1).
    1.4. For each discrete boundariness point
        1.4.1 Compute initial medialness at the location of its contribution using the LUT (Fig. 6) and Eq. (12).
        1.4.2 Compute contribution confidence for each boundariness point using Eq. (6) and Eq. (8).
    1.5. For each discrete medialness point accumulate the revised contributions using the LUT (Fig. 6) and Eq. (15).

Figure 3: Outline of CMAT algorithm

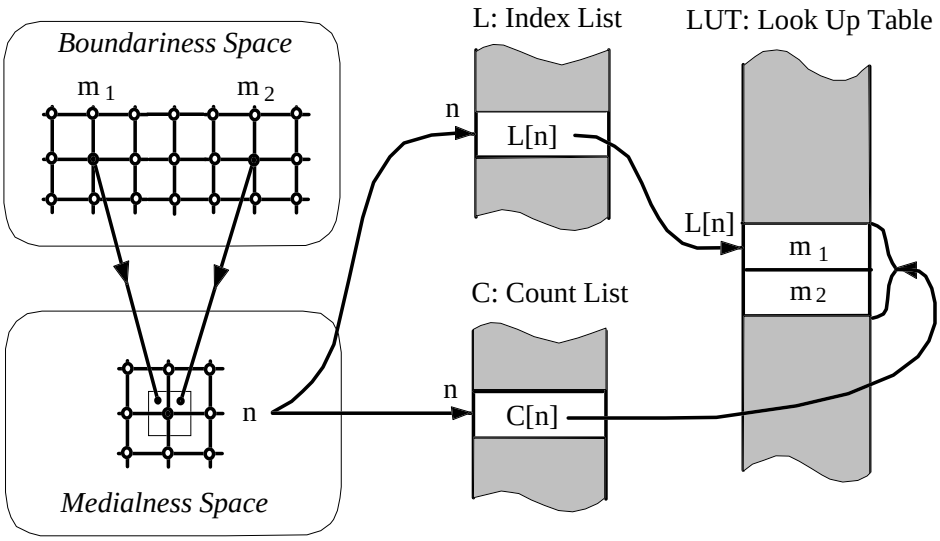

Figure 4: The structure of the look-up table for associating medialness and boundariness points.

2.1.3.1 Association of medialness and boundariness points

Although medialness response is the accumulation of co-ordinated boundariness contributions, only a few boundariness points are relevant to the computation of each medialness value. A look-up table (LUT) is used to identify the boundariness points that satisfy $\delta_p(\mathbf{n}-\mathbf{m}-r\hat{\mathbf{n}}(\mathbf{m},\sigma))=1$, and are therefore relevant at each scale.

Suppose that there are N points in boundariness and medialness space. Then an N-element LUT (see Fig. 4), organised into N groups and indexed by medialness position n (n=1,…,N) will describe the association between medialness and boundariness points. A group, n, is the set of the boundariness points whose contributions are closest to medialness grid point n. The content of the LUT is the position, m, of the boundariness points. The start position and count of each group are recorded in arrays L and C, respectively. If group n is empty, its start position coincides with that of the next medialness point. The creation of the LUT is described in Fig.5.

Definitions: m grid point co-ordinates in boundariness space; m=1, …, N.

n grid point co-ordinates in medialness space; n=1, …, N

L[n] the start address of group n in the LUT.

C[n] the counter of group n in the LUT

LUT[i] the content of LUT indexed by i; i=0,…,N-1.

Y[m] the co-ordinates of the medialness point associated with boundariness point m.

1. For each discrete point, n (n=1,…N), in medialness space, set group counter C[n]=0.
2. For each discrete point, m, in boundariness space
   - 2.1 Compute the real-valued position, y, of its contribution in medialness space using Eq. (4).
   - 2.2 Find the grid point, n, in medialness space that is closest to y.
   - 2.3 Y[m]=n;
   - 2.4 C[n]=C[n]+1.
3. L[1]=0.
4. For successive discrete points, n, in medialness space; n=2, …, N
   L[n]=L[n-1]+C[n].
5. For each discrete point, m, in boundariness space
   - 5.1 n=Y[m].
   - 5.2 Fill in boundariness position, m, into the LUT: LUT[L[n]+C[n]-1]=m.
   - 5.3 C[n]=C[n]-1.

Figure 5: Algorithm for creation of LUT association between medialness and boundariness points.

A detailed description of how the LUT is read is given in Fig. 6.

1. For each discrete point, n, in the supporting region of medialness space:

    1.1. Compute the size of group n using C[n]=L[n+1]-L[n],

    1.2. Repeat

        1.2.1 Read the boundariness co-ordinates, m, of a member of group n from the LUT as: m=LUT[L[n]+C[n]-1].

        1.2.2 Accumulate the boundariness contribution from m.

            In step 1.4.1 of the CMAT algorithm (Fig. 3) use Eq. (12).

            In step 1.5 of the CMAT algorithm (Fig. 3) use Eq. (15).

        1.2.3 C[n]=C[n]-1.

    Until C[n]=0.

Figure 6: Reading the LUT.

2.2 The HMAT-2 Transform

This transform is an adaptation of the HMAT. It is the same as the CMAT with the concordance criteria omitted and differs from the HMAT in using a circular region for distributing boundariness contributions, rather than an arc [8]. It is presented here to demonstrate the role of the concordance criteria. The HMAT-2 medialness response is computed as a weighted summation of initial boundariness contributions over a region, that is:

$$M_0(\mathbf{n},\sigma) = \sum_{\mathbf{m}} b(\mathbf{m},\sigma) G(\mathbf{n}-\mathbf{m}-r\hat{\mathbf{n}}(\mathbf{m},\sigma), s) \qquad (17)$$

The algorithm for the HMAT-2 is the same as that for the CMAT but without step 1.4.

3 THE CONCORDANCE PROPERTY

3.1 Concordance Factor

Suppose *N* points contribute to a medial point A; that the boundariness responses at these points are $b_i, i = 1,\ldots, N$; the sum of these boundariness values is *S* and the average is $\bar{b}$.

The medialness estimate at point A, without considering the relation among b_i, (as computed in the HMAT) is:

$$M_{HMAT}(\mathbf{x}_A, \cdot) = S \tag{18}$$

For the CMAT, the confidence of contributions to a true medial structure is $1 - \frac{b_i}{S}$, for each point b_i. Therefore the medialness response is:

$$M_{CMAT}(\mathbf{x}_A, \cdot) = \sum_{i=1}^{N} b_i (1 - \frac{b_i}{S})$$

$$= S - \frac{1}{S}\sum_{i=1}^{N} b_i^2 \tag{19}$$

Examining $\sum_{i=1}^{N} b_i^2$, we have,

$$\sum_{i=1}^{N} b_i^2 = \sum_{i=1}^{N} (b_i - \bar{b})^2 + N\bar{b}^2$$

$$= \sum_{i=1}^{N} (b_i - \bar{b})^2 + \frac{S^2}{N} \tag{20}$$

$\sum_{i=1}^{N} b_i^2$ has minimum value $\frac{S^2}{N}$ when:

$$b_i = \bar{b} = \frac{S}{N}, \quad i = 1,\ldots, N \tag{21}$$

For the maximum value of $\sum_{i=1}^{N} b_i^2$, there are two cases to be considered:

(1) More than one boundary point contributes to the medialness at A,

i.e. $b_i < S, \quad i = 1,\ldots,N$,

$$\because \quad \sum_{i=1}^{N}\left(\frac{b_i}{S}\right)^2 < \sum_{i=1}^{N}\frac{b_i}{S} = 1$$

$$\therefore \quad \sum_{i=1}^{N} b_i^2 < S^2$$

(2) Only one boundary point contributes to the medialness at A, i.e. :

$$b_k = S;\ b_i = 0,\ i = 1,\ldots,N \text{ and } i \neq k \tag{22}$$

$$\therefore \quad \sum_{i=1}^{N} b_i^2 = S^2$$

Therefore $\sum_{i=1}^{N} b_i^2$ has maximum value S^2 when Eq. (22) is satisfied; and $\sum_{i=1}^{N} b_i^2$ is constrained between:

$$\frac{S^2}{N} \le \sum_{i=1}^{N} b_i^2 \le S^2 \tag{23}$$

Combining Eq. (20) and Eq. (23), we have:

$$0 \le \sum_{i=1}^{N} (b_i - \bar{b})^2 \le S^2\left(1 - \frac{1}{N}\right) \tag{24}$$

Let:

$$c = \begin{cases} 1 - \dfrac{\sum_{i=1}^{N} (b_i - \bar{b})^2}{S^2\left(1 - \frac{1}{N}\right)} & N > 1 \\ 0 & N = 1 \end{cases} \tag{25}$$

Then the medialness response of the CMAT in Eq. (19) can be written as:

$$M_{CMAT}(\mathbf{x}_A,\cdot) = S - \frac{1}{S}\left[\sum_{i=1}^{N}(b_i - \bar{b})^2 + \frac{S^2}{N}\right]$$

$$= \left(1 - \frac{1}{N}\right)Sc \tag{26}$$

Note that c can also be written as:

$$c = \begin{cases} 1 - \dfrac{\sum_{i=1}^{N}(b_i - \bar{b})^2 \Big/ (N-1)}{S^2/N} & N > 1 \\ 0 & N = 1 \end{cases} \tag{25a}$$

The item $\sum_{i=1}^{N}(b_i - \bar{b})^2 \Big/ (N-1)$ is the sample variance, a measure of the dispersion, of the N observations, b_i, normalised by S^2/N, the largest value of the dispersion (see Eq. (24)). Therefore c measures the dispersion or variability of the contributions. The smaller the amount of variability, the greater the value of c and the more concordance there is among the contributions. Thus c is called the concordance coefficient. We note that $0 \le c \le 1$. When $c = 0$ Eq. (22) is satisfied, which is equivalent to there being only one boundary point casting its contribution to point A and there being no concordance. When $c = 1$ Eq. (21) is satisfied, which corresponds to N equal-valued contributions combining to give the maximal degree of concordance [19].

The CMAT medialness response in Eq. (26) is proportional to the sum of boundariness responses and to the concordance coefficient among the boundariness responses. In addition when $c = 1$ the medialness responses of the CMAT are smaller than those of HMAT by a factor $1 - (1/N)$. This factor is related to the number of boundary points involved in a

symmetry. Therefore the CMAT medialness response at end points and branch points is enhanced. A similar behaviour is present in the HMAT medialness response. Morse [8] pointed out that such enhancement is beneficial because it more clearly identifies the end and branch points that best define the axis.

3.2 Boundariness Response versus Concordance

The medialness response of the CMAT is proportional to both the sum of boundariness responses and the concordance between boundariness responses. It is therefore important to consider the interaction of these two factors. Consider the idealised situation, shown in Fig. 7, of Gaussian boundariness responses for two step edges that differ in magnitude. The boundariness responses at A and B are the local maxima with the magnitudes of V and U respectively ($U>V$). C is the position at which the boundary response due to the edge at B is equal to the maximum response of the edge at A. Suppose that positions E and D are the midpoints of AC and AB respectively, and that the half distances of AC and AB are $k\sigma_1$ and $k\sigma_2$, respectively. Here k is the ratio of radius to scale.

Since:

$$M_{HMAT}(\mathbf{x}_E, \sigma_1) = B(\mathbf{x}_A, \sigma_1) + B(\mathbf{x}_C, \sigma_1) = 2V$$
$$M_{HMAT}(\mathbf{x}_D, \sigma_2) = B(\mathbf{x}_A, \sigma_2) + B(\mathbf{x}_B, \sigma_2) = U + V$$

Then: $$M_{HMAT}(\mathbf{x}_D, \sigma_2) > M_{HMAT}(\mathbf{x}_E, \sigma_1).$$

By inspection it is clear that the HMAT will produce a maximal medialness response at position D, the medial position between the peaks of boundariness response, and give an accurate identification of medial position and object width. For the CMAT the concordance between the boundariness responses at positions A and B (which determine the medialness

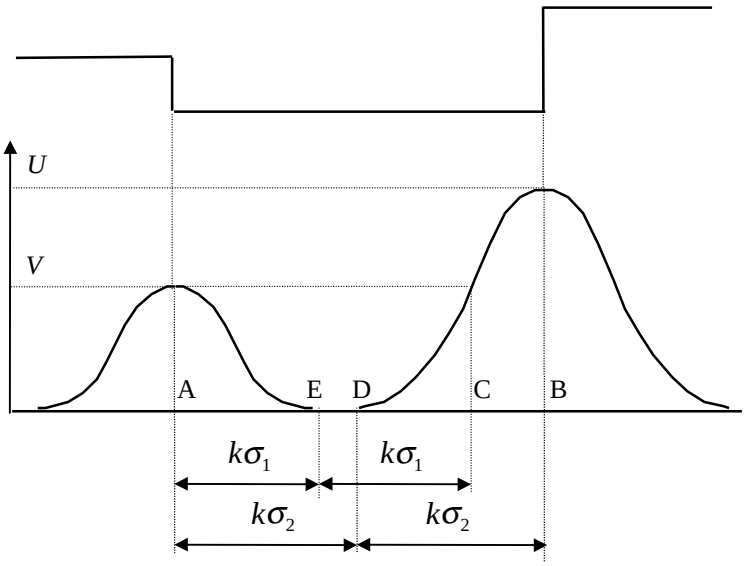

Figure 7: Interaction of boundariness strength and concordance in estimating medialness response.

response at D) is weaker than the concordance between the boundariness responses at positions A and C (which determine the medialness response at E). However, the boundariness sums at D and E bear the inverse relationship therefore it is difficult to compare, in a simple manner, the relationship between the medialness responses at D and E.

In order to estimate how concordance influences the way in which boundariness contributes to medialness we analyse incremental changes in CMAT medialness. Suppose, as in the previous section, that *N* points in boundariness space contribute to a medial point; that the boundary response at these points is $b_i, i = 1,\ldots, N$; and that the summation of these responses is *S*. Then the CMAT medialness response is defined by Eq. (19).

If any one boundariness response, b_k, is increased by Δb_k, then the summation is increased to $S + \Delta b_k$ and increment in CMAT medialness response is:

$$\Delta M_{CMAT}(\cdot,\cdot) = \frac{\sum_{i=1}^{N} b_i^2 - 2Sb_k + S^2}{S} \cdot \frac{\Delta b_k}{S + \Delta b_k} \tag{27}$$

Let:
$$T = \frac{\sum_{i=1}^{N} b_i^2 - 2Sb_k + S^2}{S} \tag{28}$$

using $\sum_{i=1}^{N} b_i^2 = b_k^2 + \sum_{\substack{i=1 \\ i \neq k}}^{N} b_i^2$, then:

$$T = \frac{\sum_{\substack{i=1 \\ i \neq k}}^{N} b_i^2 + (S - b_k)^2}{S} \tag{28a}$$

Note that item T is not related to the increment Δb_k. If we treat all initial boundary responses as constant then T is also a constant. Note also that $T = 0$ only when $b_i = 0, i = 1, \ldots, N \text{ and } i \neq k$, this corresponds to one boundariness point contributing to the medialness value. In this case, no CMAT medialness response will be produced. In the case of multiple boundariness elements, $T > 0$, will there be an increase of boundariness response resulting in an increase in medialness response.

With the HMAT, the medialness increment due to increased boundariness response, Δb_k is:

$$\Delta M_{HMAT}(\cdot,\cdot) = \Delta b_k \tag{29}$$

If the original boundary responses are treated as constants, the increment of the HMAT and CMAT medialness responses change with the ratio:

$$\beta = \frac{\Delta b_k}{S} \tag{30}$$

Here β may be considered as the relative increment in boundariness. With this definition, the

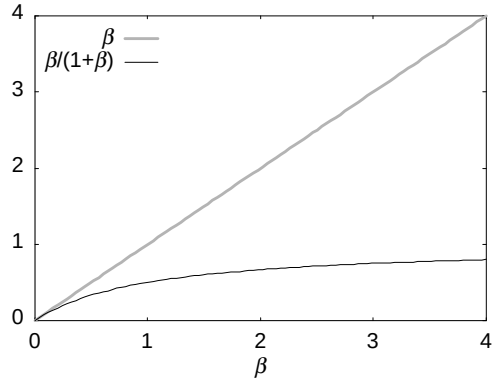

Figure 8: β and $\beta/(1+\beta)$ vs. β. Increment of HMAT and CMAT medialness related to boundariness increment.

HMAT and CMAT medialness increment can be written as:

$$\Delta M_{HMAT}(\cdot,\cdot) = S\beta \tag{31}$$

$$\Delta M_{CMAT}(\cdot,\cdot) = T\frac{\beta}{1+\beta} \tag{32}$$

Therefore the medialness increment for the HMAT and CMAT depend on the behaviour of the two coefficients β and $\frac{\beta}{1+\beta}$. The relationship between β and $\frac{\beta}{1+\beta}$ as a function of β, is shown in Fig. 8. In summary:

1. The medialness of the CMAT, like that of the HMAT, increases monotonically with boundariness**.** The CMAT forms a maximal response at positions midway between peaks of boundariness response and the magnitude of the medialness peak is in proportion to the magnitude of the contributing boundariness peaks. Therefore medial position and object width can be identified as accurately using the CMAT algorithm as the HMAT algorithm.
2. While the HMAT medialness increases linearly with boundariness increment, the increase in CMAT medialness is less than that for the HMAT and approaches the

limiting value of T. For example when $\beta = 1$, according to the definition in Eq. (30), $\Delta b_k = S$; In this case one boundariness response, b_k, becomes much larger than any other and therefore violates the previously computed concordance level; When $\beta = 1$ the coefficient $\beta / (1+\beta)$, in the CMAT medialness increment of Eq. (32) is decreased to half the value of the coefficient, β, used in the equation for the increase in HMAT. This means that weak concordance among boundary responses restrains the increase in medialness response that arises when the boundariness response is strong.

4 PERFORMANCE

4.1 Medialness Distribution in Scale Space

To obtain quantitative estimates of the performance of the CMAT algorithm we have applied the LoG, HMAT and CMAT medialness algorithms to the 1-D object profile, shown in Fig. 9(a). This profile corresponds to a dark "object" on a brighter background. The height of the right edge is double that of the left edge. Although the quantitative relation between the heights of these two edges is arbitrary, the notion of varying boundary strength in grey-level images is represented. In these experiments spatial position is normalised by "object radius" (half-distance between edges). Each medialness response is sensitive to both polarities of boundary transition and is normalised by the maximum of the medialness response over scale.

In n-dimensional co-ordinate space, the LoG medialness operator can be expressed as:

$$\begin{aligned} K(\mathbf{x},\sigma) &= -\sigma^2 \nabla^2 G(\mathbf{x},\sigma) \\ &= \frac{1}{(2\pi\sigma^2)^{n/2}} \left(n - \frac{\mathbf{x}^T\mathbf{x}}{\sigma^2} \right) e^{-\mathbf{x}^T\mathbf{x}/2\sigma^2} \end{aligned} \tag{33}$$

where **x** is the multi-dimensional co-ordinate vector.

The positive portion of the LoG operator is within a distance of $\sqrt{n}\sigma$ from the centre of this operator. At a given scale, σ, the LoG operator gives the strongest response for objects with a radius of $\sqrt{n}\sigma$; The HMAT and CMAT give the strongest response for objects with a radius of $k\sigma$. To compare these responses over scale, the radius of the operator is used as a base parameter. The radius of the LoG operator is defined as $r = \sqrt{n}\sigma$. The radius of the HMAT and CMAT operators is defined as $r = k\sigma$. These medialness operators may respond optimally to an object at different scales (the standard deviation of the Gaussian), but should

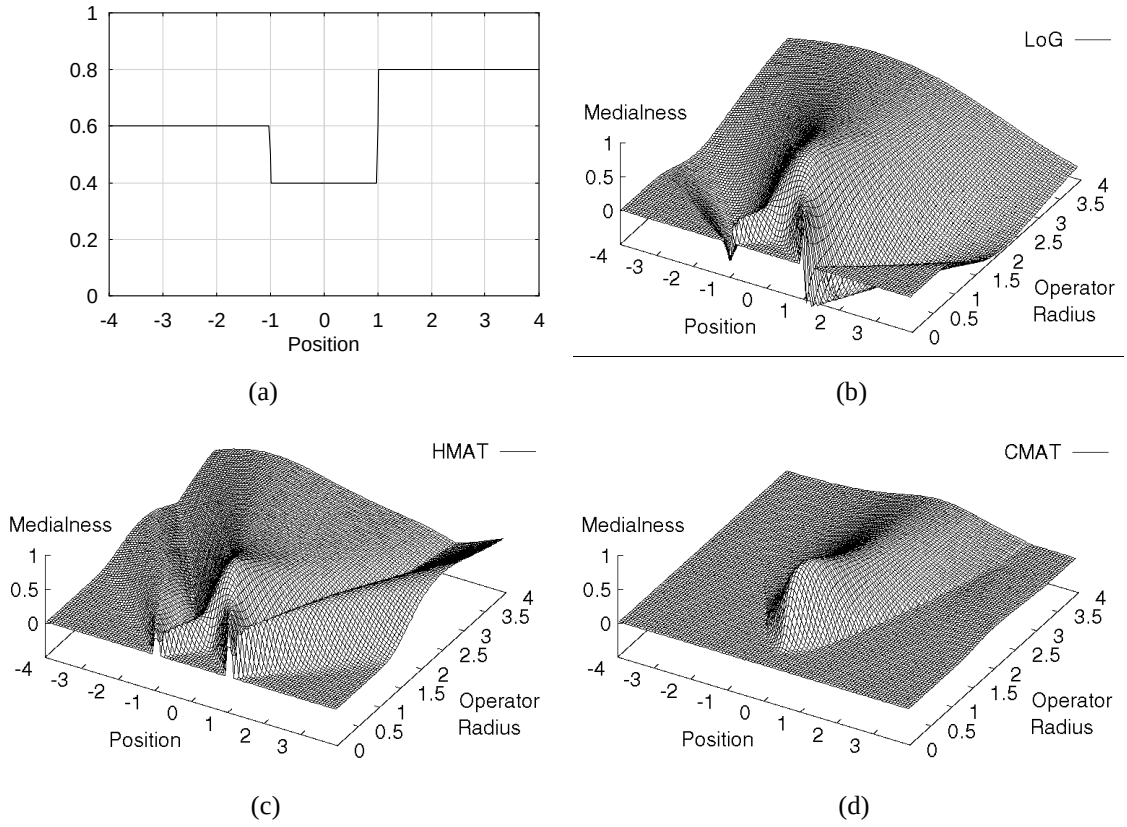

Figure 9: A 1-D object profile (a), and its scale-space surface of medialness from the LoG (b), HMAT (c) and CMAT (d). The minimum operator radius is 0.04.

respond optimally at the same operator radius. Here the scale factor that determines operator radius, *k*, is set at 2. The Gaussian weighting in Eq. 13 is not used because the sampling interval of operator radius is selected to multiple the sampling interval of spatial position and therefore in 1-D case each boundariness contribution is located at a discrete medialness point.

Figs. 9(b)-(d) show the 2-D scale-space surface of the LoG, HMAT and CMAT medialness responses for the 1-D object profile in Fig. 9(a). The increment and minimum value of operator radius is 0.04. Each medialness response forms a maximum at the position of the object centre and at the radius of the object. However, the medialness scale-spaces of the LoG and HMAT are a mixture of boundary and medial properties, while that of the

CMAT reflects only medial properties and therefore provides a clearer description.

Figs. 10(a)-(f) show variation in LoG, HMAT and CMAT medialness response with radius. The radius was increased geometrically by a factor of 2 between each evaluation and the response for an operator radius of 0.64 was added in Fig. 10(c). The evolution of the LoG and HMAT medialness responses at increasing radii is the simple summation of boundariness response from each edge as the spread of boundariness increases with radius. At small operator radii, far from the object radius, Fig. 10(a), the medialness responses of the LoG and HMAT, caused by responses to edges, are already strong (67% of their maximum over scale) while the CMAT produces no response. As operator radius increases, Fig. 10(b), the summation of the LoG and HMAT boundariness responses produces a response which peaks away from the "object" centre. Only the CMAT produces a medialness response at the object centre. When the operator radius increases to 64% of the object radius, Fig. 10(c), the summation of the LoG and HMAT boundariness responses begins to combine into a single main lobe away from the object centre, and the CMAT medialness continues to increases at the correct position. When the operator radius matches the object radius, Fig. 10(d), all three algorithms produce their maximal responses at the object centre, but the LoG and HMAT produce two additional side-lobe responses. The curve of the CMAT medialness response coincides with the main lobe of the HMAT medialness response. When operator radius is larger than the object radius, Figs. 10(e)-(f), the medialness response of each algorithm begins to collapse and deviate, in position, from the object centre. The response of the CMAT is always enveloped in that of the HMAT, and the response of the HMAT is enveloped in that of the LoG, which shows that the sequence of selectivity to medial position (best first) is: CMAT, HMAT, and LoG**.** At an operator radius other than the object radius, the peak position

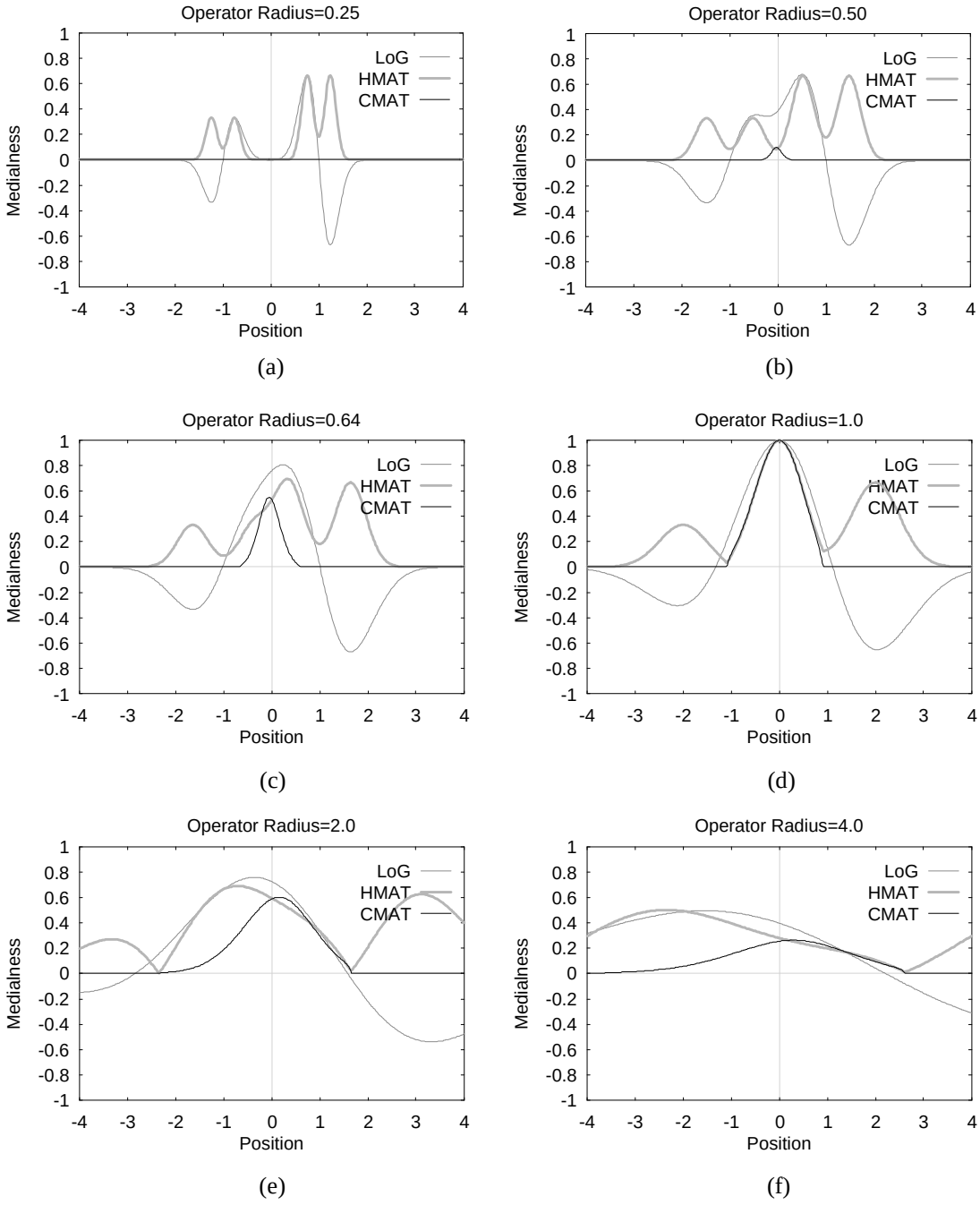

Figure 10: The LoG, HMAT, and CMAT medialness responses as a function of position and at selected operator radii.

of the CMAT medialness is much closer to the object centre than is the response for the HMAT and LoG algorithms.

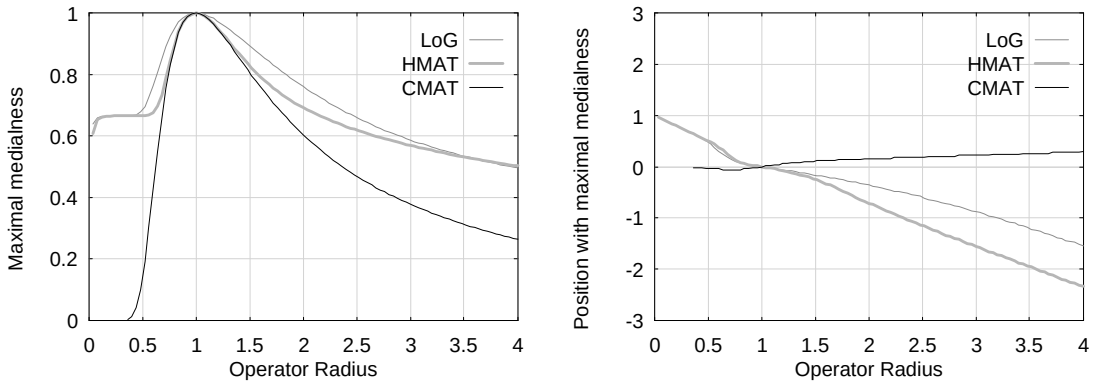

(a) (b)

Figure 11: The magnitude (a) and position (b) of medialness maxima, with respect to position, at a range of operator radii for the LoG, HMAT, and CMAT algorithms.

Fig. 11(a) shows the maximal medialness response as a function of operator radius for the LoG, HMAT and CMAT. Each transform gives a maximal response when the operator radius matches the object radius. Therefore we can accurately localise the object radius using any of these algorithms. The sequence of selectivity to the object radius (best first) is: CMAT, HMAT and LoG.

Fig. 11(b) shows the locus of medialness maxima with respect to position at a range of operator radii for the LoG, HMAT and CMAT. Each trace crosses the object centre when the operator radius matches the object radius, and deviates from the object centre almost linearly as operator radius increases. Therefore we can accurately localise the object centre using any of these algorithms. The sequence of precision in spatial localisation for these operators at a range of operator radii (best first) is: CMAT, LoG and HMAT. When operator radius is four times the object radius, the localisation bias of object centre for the CMAT is 13% that for the HMAT and 19% that for the LoG. The HMAT medialness response is more readily moved to one side by differences in boundary strength than the LoG medialness. This result is contrary

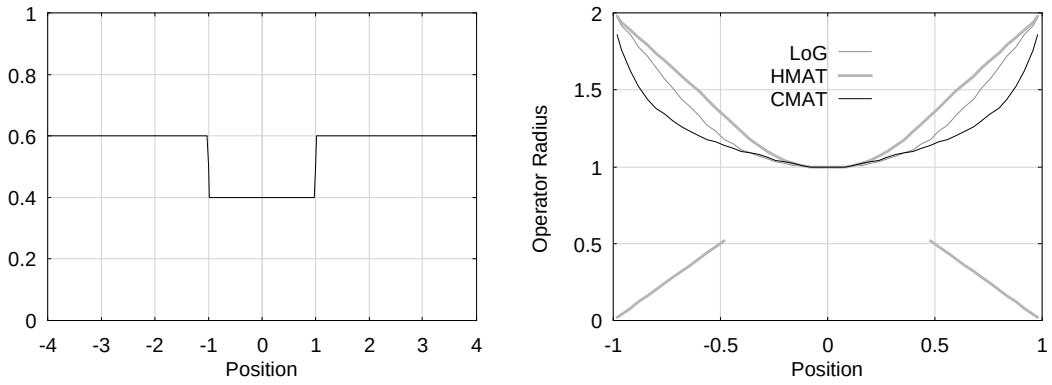

(a) (b)

Figure 12: A 1-D object profile (a) and loci of medialness maxima with respect to radius at a range of positions (b).

to the observation in [8][9] concerning the behaviour of axis-centred medialness operators (LoG) and boundary-centred operators (HMAT).

In order to identify “the optimal scale ridge” for medial axis extraction, medialness maxima with respect to scale at each spatial position are located [4][13]. The set of these maxima are a set of curves for 1-D objects and surfaces for 2-D objects. Fig. 12(b) shows the loci of the LoG, HMAT and CMAT medialness maxima with respect to operator radius at a range of positions along the 1-D object of Fig. 12(a); The two edges of the object have the same height. At positions away from the object centre, the LoG, HMAT and CMAT medialness responses exhibit maxima at an operator radius larger than the object radius. The sequence of localisation of object radius at a range of positions (best first) is: CMAT, LoG and HMAT. When the position is within 80% of the object radius, the localisation bias of object radius for the CMAT is under 50% of that for the HMAT. At the boundary each maxima locus occurs at an operator radius double the object radius. For positions near to the boundary, the LoG and HMAT responses contain two maxima, while the CMAT response has

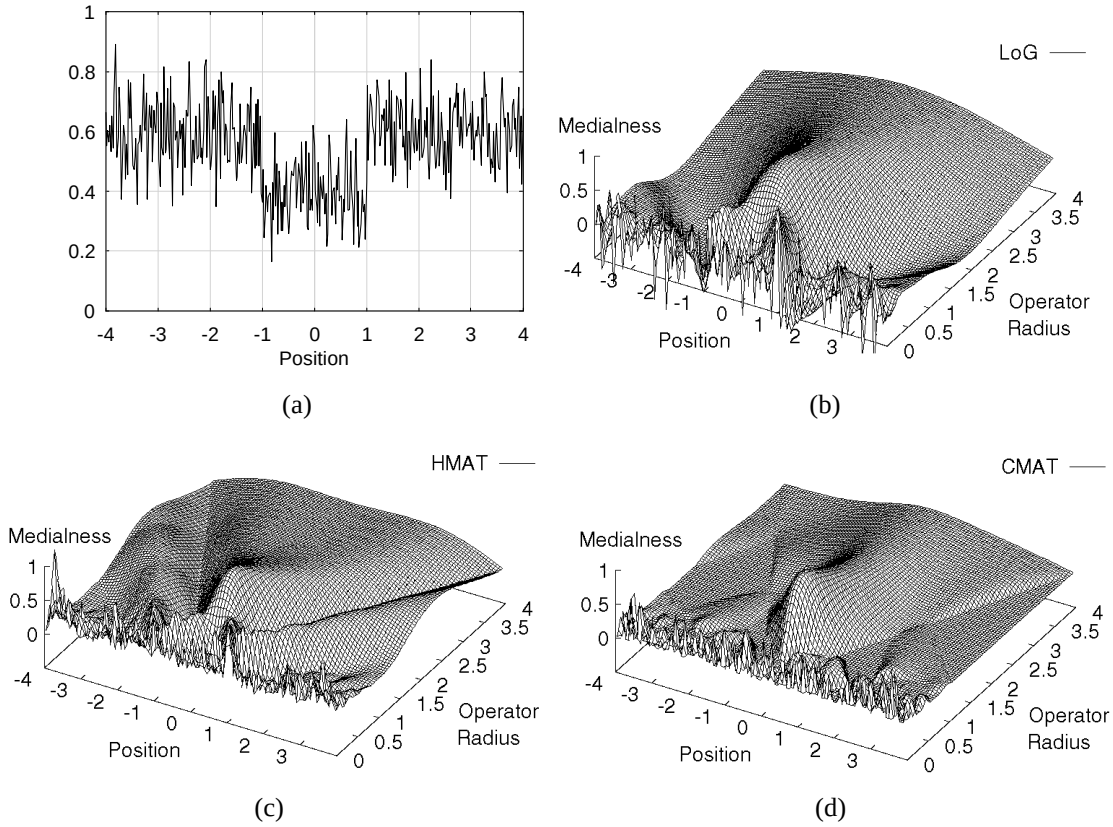

Figure 13: A 1-D object profile with noise added (SNR=2) (a), and the scale-space surface of medialness for the LoG (b), HMAT (c) and CMAT (d) algorithm.

only one maxima. Not all spatial positions have a single medialness maxima as a function of scale because a single spatial position may be in different medial axes at multiple radii. However for this single structure, the maxima locus of the LoG and HMAT responses at smaller operator radii does not represent any symmetry and is an artefact.

4.2 Effect of Noise on Medialness Computation

We have tested the LoG, HMAT and CMAT algorithms using a 1-D object profile with added white Gaussian noise to investigate the noise sensitivity of the localisation of medialness response in spatial position and scale. Fig. 13(a) shows an object profile similar to

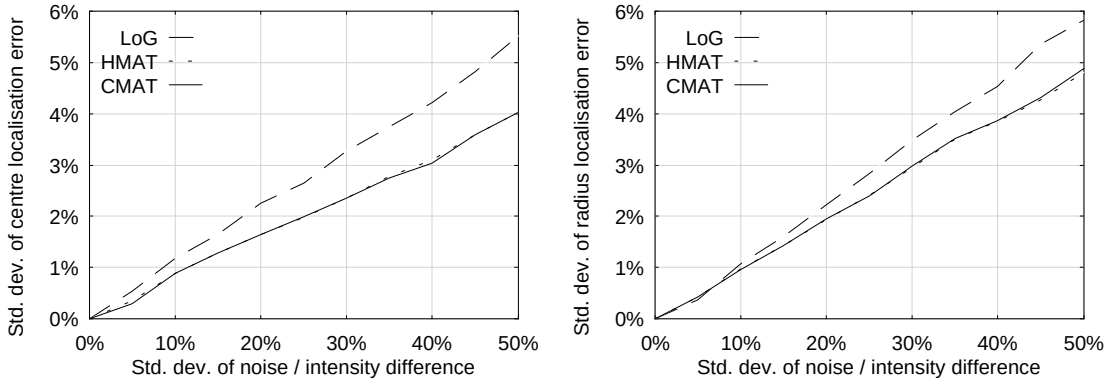

(a) (b)

Figure 14: The standard deviation in localisation of object centre (a) and object radius (b) under increasing noise levels.

that shown in Fig. 12(a) but with zero-mean, Gaussian-distributed noise added. The standard deviation of this noise is 50% of the signal amplitude.

Figs. 13(b)-(d) show the 2-D scale-space surfaces of the medialness response for the LoG, HMAT and CMAT applied to the profile shown in Fig. 13(a). Each medialness response forms a maximum for the object near the position of the object centre and at a radius close to object radius. At low noise levels, the medialness response was altered at small radii only. As the level of noise was increased, the response at larger radii was affected. The response surface for the LoG is smoother than that of the HMAT and CMAT, This is likely to be due to the larger smoothing operator used in the LoG algorithm.

Figs. 14(a) and (b) show the standard deviation of localisation errors of object centre and object radius for the LoG, HMAT and CMAT, respectively, under increasing noise levels. They are computed using 1,000 profiles at each noise level. The object centre is realised as the maximal medialness point with a spatial position in the range [-0.5,0.5] and a radius in the range [0.7,1.5]. The results show that the standard deviation of localisation error for object centre and object radius for the LoG, HMAT and CMAT all increase linearly with the

standard deviation of noise level. The curves for the CMAT coincide with those for the HMAT, which shows again that these two algorithms perform similarly near the position of the object centre and the object radius. The HMAT and CMAT are 27% lower in object centre localisation error and 15% lower in object radius localisation error than the LoG. This is consistent with Morse's conclusion [9] that axis-centred operators, like the LoG, are sensitive to variations within the object because they require integration over the entire width of the object.

4.3 Application to 2-D Images

To assess the significance of the results presented above we evaluated the CMAT algorithm using synthetic and natural images. We compared these results with the results that we obtained using our own implementations of the LoG, HMAT and credit attribution algorithm. The linear HMAT was used throughout this paper. The results for the HMAT-2, the initial medialness response of the CMAT, is also provided to demonstrate how the improved CMAT responses arises. The size of each image is 128×128 pixels. Each medialness operator is sensitive to both polarities of boundary transition. The medialness images show the absolute value of medialness response. Therefore in the medialness results for the LoG operator the zero-crossings, which reflect boundary information, are replaced by minima with zero value. As in the 1-D case, we use operator radius as a common parameter of scale between the operators. Here the scale factor that determines operator radius, k, is set at 2 and the scale factor that determines the extent of the boundariness distribution, λ, is set at 0.5.

Fig. 15 shows the medialness responses for a rectangle with a sawtooth edge. For the LoG (first row) and HMAT (second row) operators, "spurious" medial responses appear as lines

framing the shape; the brightest regions correspond to true medial responses. At a radius of 5 and 10 pixels, the "spurious" responses are mainly caused by the sensitivity of a linear operator to edges. At a radius of 20 pixels, the response of both linear operators consists of a central medial response the ridge of which provides a precise description of the overall shape, and an outer "spurious" structure due to the side-lobe effect. The credit attribution algorithm makes the true medialness response more prominent (third row). The side-lobe response present in Fig. 15(d) and (g) are eliminated. However, the credit attribution algorithm has little impact on the way that edges generate a "medialness" response (at radii of 5 and 10 pixels). This is not surprising because the enhancement of the credit attribution depends on the HMAT medialness contrast between the main and side lobes. The HMAT-2 algorithm produces a result similar to that of the HMAT (fourth row) but the medial axes are more strongly emphasised. This is due to the range of values for θ in Eq. (14) being smaller than the corresponding effective angle of distribution for the circular arc used in the HMAT algorithm [8]. With the CMAT algorithm (fifth row), only true medial responses are generated at all radii. The hierarchy and robustness of multiscale analysis are demonstrated in each set of results: the triangular sawteeth and end corners are reflected at small radii (left column), the rectangular shape is reflected at medium radii (middle column), and the elongated shape is reflected at large radii (right column); The medialness of larger scale properties is little affected by fine detail.

Fig. 16 shows the medialness responses for a teardrop shape. The radius of the circular arc at the bottom of the teardrop is 24 pixels. Therefore the radius at which the strongest medialness response should occur for this circular arc is 24 pixels. However, we find that the LoG (first row), HMAT (second row) and credit attribution algorithms (third row) begin to

produce medialness responses for the arc at smallest radius used (5 pixels, see Fig. 16(b) and (e)). Further, these responses are displaced from the arc centre by a relatively large distance and resemble boundary responses (the left and middle columns). With the CMAT algorithm, the medialness response for the circular arc appears at a radius greater than 9 pixels and at a position close to the arc centre (fifth row). This is consistent with the medialness performance demonstrated in Section 4.1 whereby the CMAT produced a medialness response only at positions near to the object centre and at radii close to the object radius.

Fig. 17 shows the medialness response for a longitudinal body MR image of a pair of legs (an image from the Visible Human Project, http://www.nlm.nih.gov/research/visible). This image was chosen as an example of natural image, in which the amplitude of the grey-level boundary varies, the shapes are relatively complex and multiple "objects" are in close proximity. The medialness responses for the LoG (first row) and HMAT (second row) can be seen to be a mixture of medial and boundary responses. The credit attribution algorithm greatly refines the result of the HMAT, but the contour of both legs is still visible (third row). In the results of the CMAT (fifth row), only those responses that reflect true symmetry are retained: the CMAT medialness reflects the bones and the fat layers (bright regions in the inner side of legs) at small radius; at medium radius the knees are emphasised; at a large radius only the major structure of the limbs is maintained. Note that the CMAT response between the legs correctly reflects a triangular shape.

For each medialness operator, the computational cost increases linearly with radius. The times taken to compute the medialness response of a 128×128 pixel image at an operator radius of 20 pixels on a SUN Ultra-2 workstation are shown in Table 1. Five iterations were used in the credit attribution (CA) algorithm. We used a LUT to compute the Gaussian and its

derivatives in all algorithms, and another LUT to compute the weighting function in the HMAT and credit attribution algorithms.

Table 1: The computation cost of medialness algorithms at one operator radius.

Algorithms	LoG	HMAT	CA	HMAT-2	CMAT
Time (seconds)	10	40	365	11	13

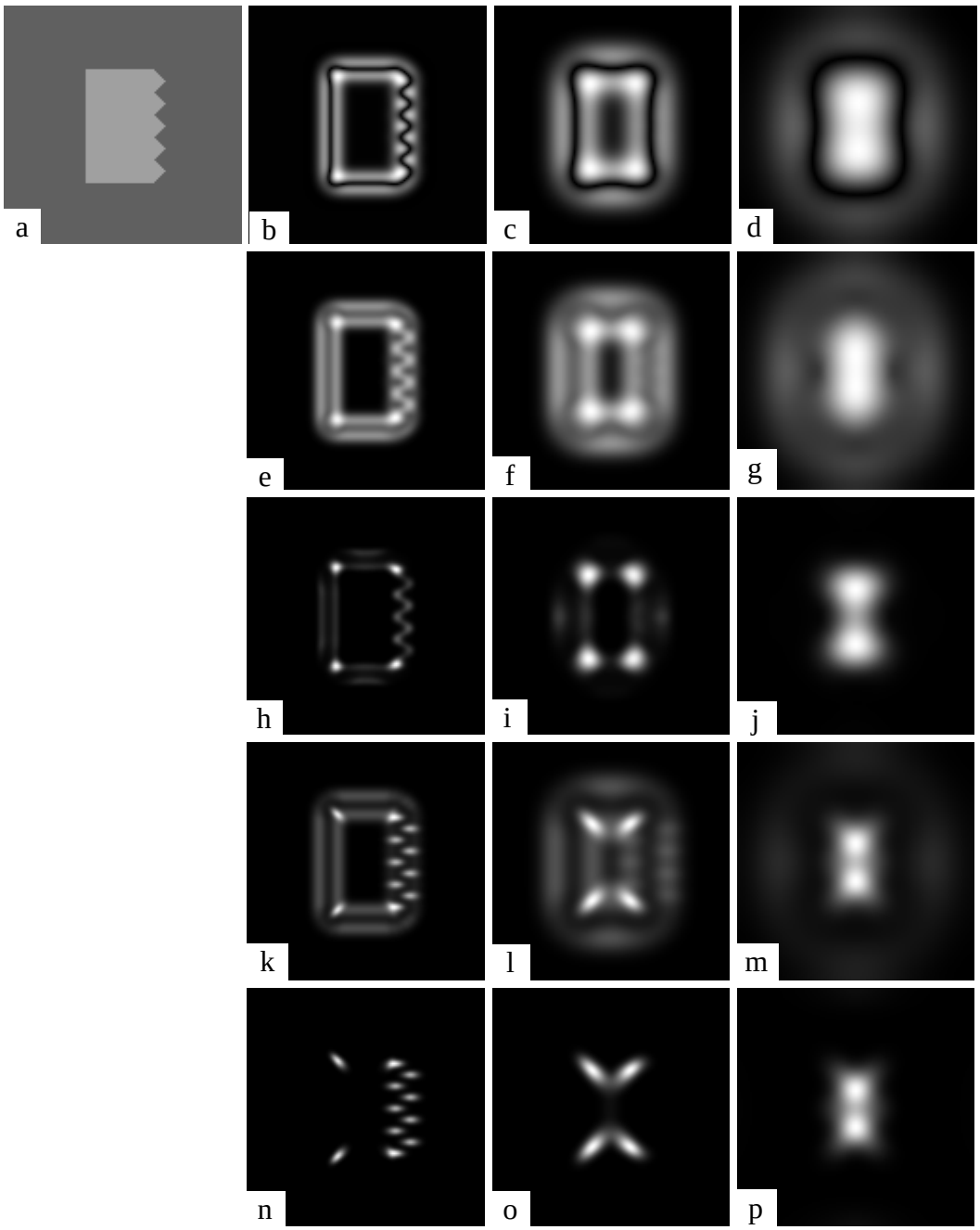

Figure 15: The medialness responses for a rectangle with a sawtooth edge: (a) Original image; first row, (b)-(d), LoG operator; second row, (e)-(g), HMAT; third row, (h)-(j), credit attribution algorithm after 5 iterations; fourth row, (k)-(m), HMAT-2; fifth row, (n)-(o), CMAT. The columns from left to right are at operator radii of 5, 10 and 20 pixels, respectively. The radius of the shape is 20 pixels.

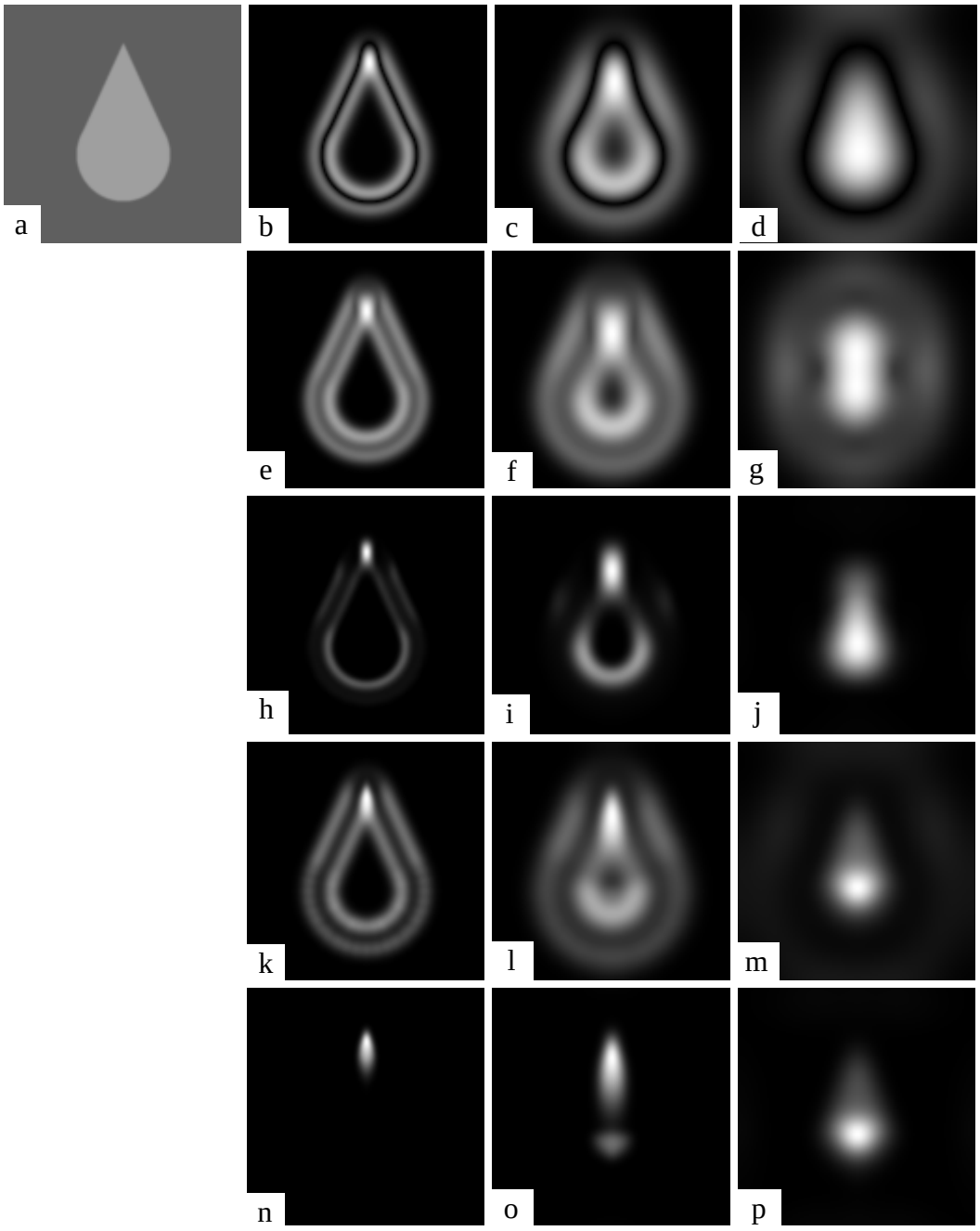

Figure 16: The medialness responses for a teardrop shape: (a) Original image; first row, (b)-(d), LoG operator; second row, (e)-(g), HMAT; third row, (h)-(j), credit attribution algorithm after 5 iterations; fourth row, (k)-(m), HMAT-2; fifth row, (n)-(p), CMAT. The columns from left to right are at operator radii of 6, 12 and 24 pixels, respectively. The radius of the circular arc at the bottom of the shape is 24 pixels.

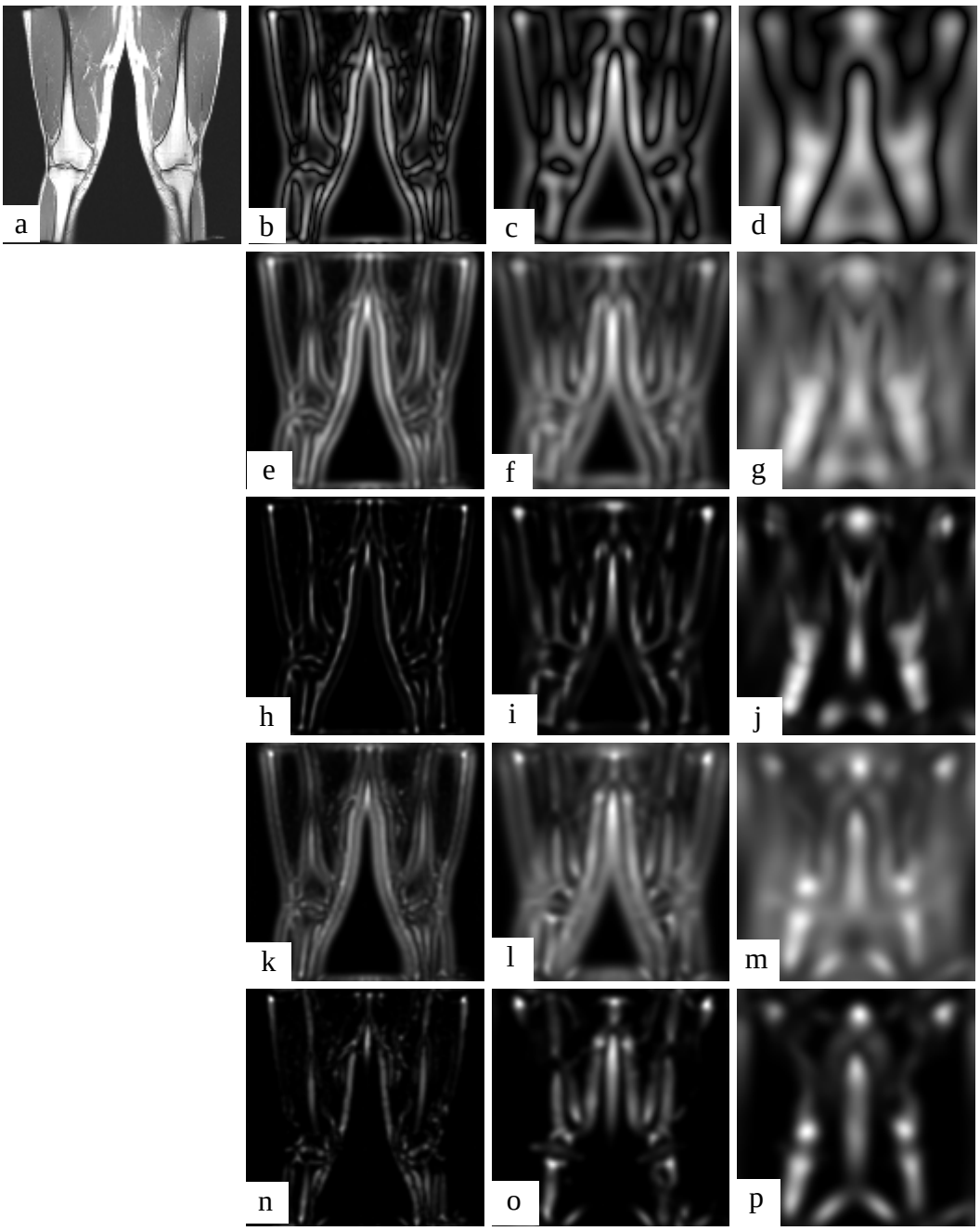

Figure 17: The medialness responses for a pair of legs: (a) Original image; first row, (b)-(d), LoG operator; second row, (e)-(g), HMAT; third row, (h)-(j), credit attribution algorithm after 5 iterations; fourth row, (k)-(m), HMAT-2; fifth row, (n)-(p), CMAT. The columns from left to right are at operator radii of 3, 6 and 12 pixels, respectively.

5 CONCLUSIONS

We have presented a non-linear algorithm, CMAT, for computing the multiscale medial response of grey-level images. For a symmetric structure, the response of this operator has only one maximum across scale-space and this maximum is at the correct scale for the width of the object. Therefore the CMAT provides a clearer description of shapes than the linear LoG and HMAT medialness algorithms which are sensitive to edges and give multiple responses to symmetric structures. This method has improved the selectivity and localisation of medial axis position and object width across scale-space. In addition, the robustness of the linear medial transforms in the presence of noise is maintained. Compared with the relaxation refinement of the linear operators [9], our algorithm is computationally more efficient. These results show that the CMAT algorithm provides a robust and computationally efficient description of symmetry in grey-level images.

APPENDIX

Alternative Definitions of Contribution Confidence

In Eq. (6), we defined the contribution confidence function, $p(\mathbf{x},\sigma)$, in the form of $f(x) = 1 - x$, where $x = b(\mathbf{x},\sigma) / m_0(\mathbf{y},\sigma)$. In general, $p(\mathbf{x},\sigma)$ is defined as a function of the ratio $b(\mathbf{x},\sigma) / m_0(\mathbf{y},\sigma)$, i. e. :

$$p(\mathbf{x},\sigma) = f[b(\mathbf{x},\sigma) / m_0(\mathbf{y},\sigma)] \tag{A1}$$

The requirements for the function $f(x)$ are:

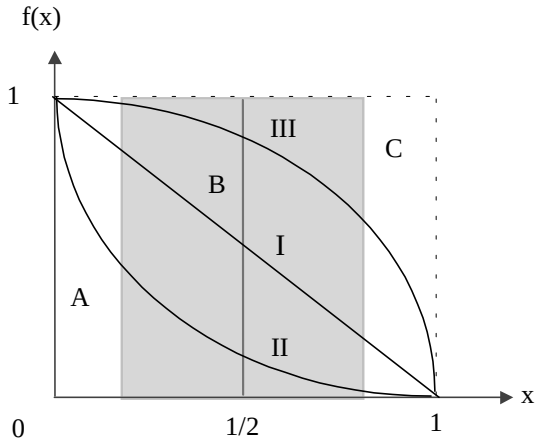

Fig. A1. Contribution confidence functions that strictly satisfy requirements of Eq. (A2).

$$\begin{aligned} &(1) \quad 0 \le f(x) \le 1, \quad 0 < x \le 1 \\ &(2) \quad f(1) = 0 \\ &(3) \quad f'(x) < 0 \end{aligned} \tag{A2}$$

Condition (1) means that the medialness response should not be greater than the initial medialness response. Condition (2) means that a single boundary point produces no medialness response. Condition (3) means that given a boundariness contribution, the greater the initial medialness, the more possible it is for this boundariness point to contribute to a true symmetric structure. These conditions constrain the values of x and $f(x)$ to the area between the coordinate axes and the dotted lines, shown in Fig. A1. This area can be divided into three regions according to the value of x:

Region A **(**$x << 1$**):** This region corresponds to situations in which boundary points cluster around an end-point, or a weak boundariness response that contributes to the initial medialness jointly with other much stronger boundariness responses.

Region C **(** $x \to 1$**):** This region corresponds to the situation in which a strong boundariness response contributes to the initial medialness jointly with other much weaker boundariness responses.

Region B: This region, centred at $x = 1/2$, corresponds to the situation in which two compatible boundaries, parallel to each other, contribute to the initial medialness.

The contribution confidence function defined in Eq. (6) corresponds to the function $f(x) = 1 - x$ represented by curve I in Fig. A1. Varying the shape of this function, without violating the requirements of Eq. (A2), will emphasise (or de-emphasise) end-point medialness with respect to the medialness arising from parallel boundaries. Curve II suppresses and curve III enhances the relative medialness arising from parallel boundaries.

If the last requirement of Eq. (A2), $f'(x) < 0$, is weakened a relationship for $f(x)$ can be defined to give greater emphasis to the medialness arising from parallel boundaries and less emphasis to the medialness arising from endpoints. Curve IV in Fig. A2 is one such function.

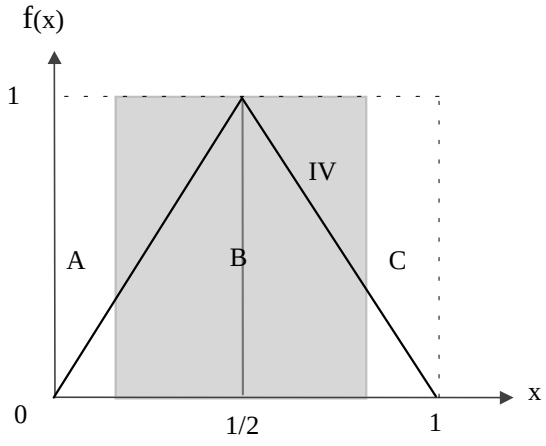

Fig. A2. A contribution confidence function that satisfies the weakened requirements of Eq. (A3).

The function of curve IV is:

$$f(x)=\begin{cases}2x & if\ 0<x\le 1/2\\ 2(1-x) & if\ 1/2<x\le 1\end{cases} \tag{A3}$$

To understand how this arises, consider the medialness for the "tube contour" shown in Fig. A3. In this figure the boundariness at each point on the contour is *b* and there are *N* points on the half-circular arc ($N >> 2$). Thus the medialness at points O (*N* contributions) and B (2 contributions, letting N=2), using Eq. (6), are:

$$\begin{aligned} M_I(\mathbf{x}_O,\cdot) &= Nb\left(1-\frac{1}{N}\right)=(N-1)b\\ M_I(\mathbf{x}_B,\cdot) &= b \end{aligned} \tag{A4}$$

Using Eq. (A3) the medialness at points O and B becomes:

$$\begin{aligned} M_{IV}(\mathbf{x}_O,\cdot) &= Nb\frac{2}{N}=2b\\ M_{IV}(\mathbf{x}_B,\cdot) &= 2b \end{aligned} \tag{A5}$$

The resulting uniform-response medialness is no longer related to the number of contributions and the medialness along the middle line of parallel boundaries is greatly enhanced. The difference in the medialness resulting from curves I and IV is similar in nature to the difference between the "mean deviation from flatness" and the "principle deviation from flatness" [4], computation of medialness. The "mean deviation from flatness" is based on the use of an isotropic convolution of a Laplacian with the image and the "principal deviation from flatness" is based on the application of a Laplacian convolution in the direction which maximises the response.

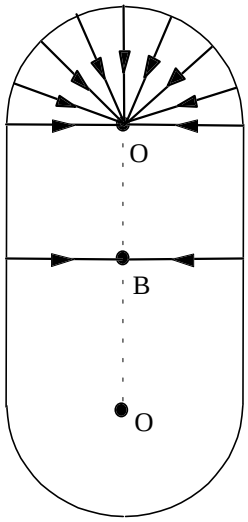

Fig. A3. Medialness accumulation from end-points and parallel boundaries.

The analyses and results presented in this paper are based on the contribution confidence $p(\mathbf{x},\sigma)$ defined in Eq. (6), in the form of $f(x) = 1 - x$ (curve I in Fig. A1).

ACKNOWLEDGEMENTS

M. Xu is funded by The University of Birmingham and the Overseas Research Students Award Scheme of the Committee of Vice-Chancellors and Principals, UK.

REFERENCES

[1] H. Blum, A transformation for extracting new descriptors of shape, in *Models for the perception of speech and vision forms* (W. Wathen-Dunn, ed.), MIT Press, 1967, pp. 362-380.

[2] J. L. Crowley and A. C. Parker, A representation for shape based on peaks and ridges in the difference of low-pass transform, *IEEE Trans. Patt. Anal. Machine Intell.*, Vol. 6, pp. 156-169, 1984.

[3] D. Eberly, R. B. Gardner, B. S. Morse, S. M. Pizer, and C. Scharlach, Ridges for image analysis, *Journal of Mathematical Imaging and Vision*, Vol. 4, pp. 351-371, 1994.

[4] D. S. Fritsch, Registration of radiotherapy images using multiscale medial descriptions of image structure, *Ph. D. Dissertation*, Dept. of Biomedical Eng., Univ. of North Carolina, 1993.

[5] R. Haralick, Ridges and valleys in digital images, *Computer Vision, Graphics, Image Processing*, Vol. 22, pp. 28-38, 1983.

[6] J. J. Koenderink and A. J. Doorn, Dynamic shape, *Biological Cybernetics*, Vol. 53, pp. 383-396, 1986.

[7] T. M. Koller, G. Gerig, G. Szekely, and D. Dettwiler, Multiscale detection of curvilinear structures in 2-D and 3-D image data, *Proc. Int. Conf. Computer Vision*, pp. 864-869, IEEE Computer Society Press, 1995.

[8] B. S. Morse, S. M. Pizer and C. A. Burbeck, A Hough-like medial axis response function, *Tech. Rep. TR91-044*, Dept. of Comp. Sci., Univ. of North Carolina at Chapel Hill, 1991.

[9] B. S. Morse, S. M. Pizer and A. Liu, Multiscale medial analysis of medical images, *Image and Vision Computing*, Vol. 12, pp. 327-338, 1994.

[10] B. S. Morse, Computation of object cores from greyscale images, *Ph.D. Dissertation*,

Dept. of Comp. Sci., Univ. of North Carolina at Chapel Hill, 1994.

[11] B. S. Morse, S. M. Pizer, D. T. Puff, and C. Gu, Zoom-invariant vision of figure shape: effects on cores of image disturbances, *Computer Vision and Image Understanding*, Vol. 69, pp. 72-86, 1998.

[12] S. M. Pizer, W. R. Oliver, and S. H. Bloomberg, Hierarchical shape detection via the multiresolution symmetric axis transform, *IEEE Trans. Patt. Anal. Machine Intell.*, Vol. 4, pp. 505-511, 1987.

[13] S. M. Pizer, C. A. Burbeck, J. M. Coggins, D. S. Fritsch and B. S. Morse, Object shape before boundary shape: scale-space medial axes, *Journal of Mathematical Imaging and Vision*, Vol. 4, pp. 303-313, 1994.

[14] S. M. Pizer, B. S. Morse, D. Eberly, and D. S. Fritsch, Zoom-invariant vision of figural shape: The mathematics of cores, *Computer Vision and Image Understanding*, Vol. 69, pp. 55-71, 1998.

[15] S. M. Pizer, D. S. Fritsch, V. E. Johnson, and E. L. Chaney, Segmentation, registration, and measurement of shape variation via image object shape, Submitted to *IEEE Trans. Med. Imaging*.

[16] I. M. Gel'fand, M. I. Graev, and N. Y. Vilenkin, Generalized functions, Vol. 5, Academic Press, New York, 1966.

[17] J. B. Subirana-Vilanova and K. K. Sung, Ridge detection for the perceptual orgnization without edges, *Proc. Int. Conf. Computer Vision*, pp. 57-64, IEEE Computer Society Press, 1993.

[18] S. Wang, A. Rosenfeld, and A. Y. Wu, A medial axis transformation for greyscale pictures, *IEEE Trans. Patt. Anal. Machine Intell.*, Vol. 4, pp. 419-421, 1982.

[19] M. Xu and D. Pycock, Estimating true symmetry in scale space, *Proc. IEEE Int. Conf. System, Man ,and Cybernetics*, pp. 4620-4625, 1998.